Electronic Supplementary Information

Quinazoline-based thermally activated delayed fluorescence emitters for high-performance organic light-emitting diodes with external quantum efficiencies about 28%

*Pan Li,[a] Yepeng Xiang,[b] Shaolong Gong,[*b] Wei-Kai Lee,[a] Yu-Hsin Huang,[a] Chun-Yu Wang,[a] Chuluo Yang*[bc] and Chung-Chih Wu [*a]*

[a] Department of Electrical Engineering, Graduate Institute of Photonics and Optoelectronics and Graduate Institute of Electronics Engineering, National Taiwan University, Taipei 10617, Taiwan.
E-mail: wucc@ntu.edu.tw
[b] Department of Chemistry, Hubei Key Lab on Organic and Polymeric Optoelectronic Materials, Wuhan University, Wuhan 430072, P. R. China.
E-mail: slgong@ntu.edu.cn; clyang@whu.edu.cn
[c] Shenzhen Key Laboratory of Polymer Science and Technology, College of Materials Science and Engineering, Shenzhen University, Shenzhen 518060, P. R. China

General information:

All reagents were used as received from commercial sources unless otherwise stated. Tetrahydrofuran and toluene were dried by sodium-potassium alloy. ^{1}H NMR and ^{13}C NMR spectra were measured on a Bruker Advanced II (400 MHz) spectrometers or MERCURYVX300. High-resolution mass spectra (HRMS) were measured on a LCQ-Orbitrap Elite (Thermo-Fisher Scientific, Waltham, MA, USA) mass spectrometer. Thermogravimetric analysis (TGA) was undertaken with a NETZSCH STA 449C instrument. The thermal stability of the samples under a nitrogen atmosphere was determined by measuring their weight loss while heating at a rate of 10 ^{o}C min $^{-1}$ from 25 to 600 ^{o}C. Cyclic voltammetry (CV) was carried out in nitrogen-purged dichloromethane (DCM) at room temperature with a CHI voltammetric analyser. Tetrabutylammonium hexafluorophosphate ($TBAPF_6$) (0.1 M) was used as the

supporting electrolyte. The conventional three-electrode configuration consists of a platinum working electrode, a platinum wire auxiliary electrode, and an Ag wire pseudo-reference electrode with ferrocenium–ferrocene (Fc^+/Fc) as the internal standard. Cyclic voltammograms were obtained at a scan rate of 100 mV s^{-1}. Formal potentials are calculated as the average of cyclic voltammetric anodic and cathodic peaks.

Experimental section:

10-(4-(quinazolin-4-yl)phenyl)-10*H*-phenoxazine (2H-Qz): To a mixture of 10-(4-(4,4,5,5-tetramethyl-1,3,2-dioxaborolan-2-yl)phenyl)-10*H*-phenoxazine (462 mg, 1.2 mmol), 4-chloroquinazoline (164 mg, 1 mmol), potassium carbonate (276 mg, 2 mmol) and Pd(PPh_3)$_4$ (5 mg, 0.005 mmol) was added 20 mL of degassed tetrahydrofuran and 10 mL of degassed water. After stirring at 80 ^oC under a nitrogen atmosphere for 24 h, the mixture was cooled down to room temperature and mixed thoroughly with 3 × 20 mL of dichloromethane. The collected organic phase was washed with water and dried with anhydrous Na_2SO_4. After filtration and removal of the solvent, the residue was purified by column chromatography on silica gel (eluent: petroleum /dichloromethane = 2:1, v/v) to afford the title compound as bright yellow powder (251 mg, yield: 65%). ^{1}H NMR (400 MHz, $CDCl_3$-*d*, 298 K) δ [ppm]: 9.44 (s, 1H), 8.23 (d, *J* = 7.9 Hz, 1H), 8.20 (d, *J* = 8.4 Hz, 1H). 8.05 (d, *J* = 8.3 Hz, 2H), 7.99 (ddd, *J* = 8.4, 7.0, 1.3 Hz, 1H), 7.71 (ddd, *J* = 8.6, 7.0, 1.0 Hz, 1H), 7.59 (d, *J* = 8.3 Hz, 2H), 6.80-6.59 (m, 6H), 6.07 (d, *J* = 8.5 Hz, 2H). ^{13}C NMR (100 MHz, $CDCl_3$-*d*, 298 K) δ [ppm]: 167.45, 154.50, 150.95, 144.24, 144.11, 137.18, 134.16, 133.87, 132.78, 131.32, 131.15, 128.22,

126.82, 123.31, 123.00, 121.72, 115.72, 115.66. HRMS (m/z): calcd for $C_{26}H_{18}N_3O^+$ $[M + H]^+$ 388.1444, found 388.1443.

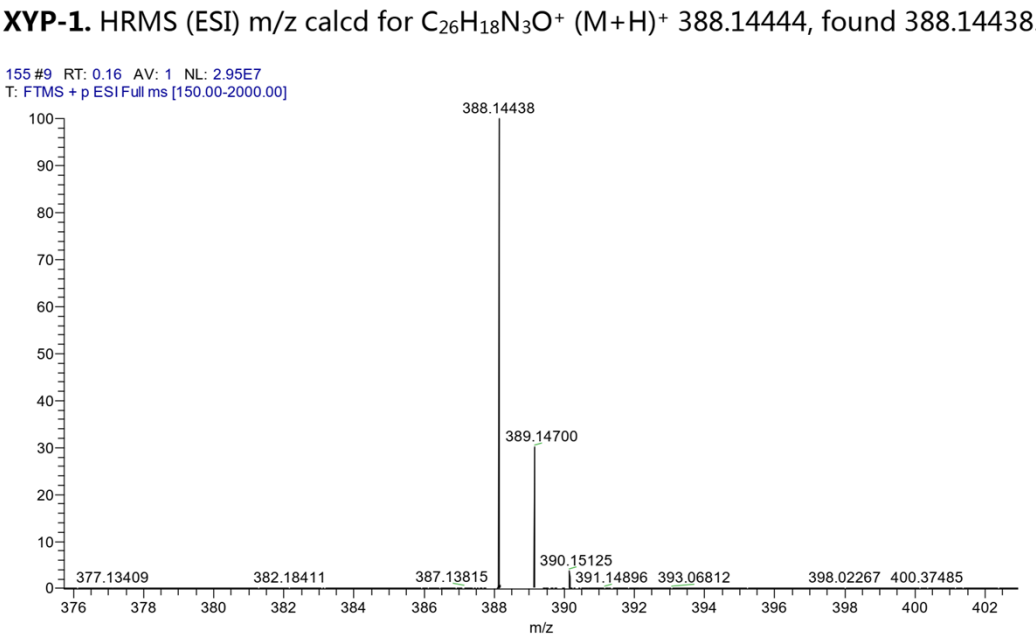

Fig. S1 HRMS (ESI) m/z calcd for $C_{26}H_{18}N_3O^+$ $(M+H)^+$ 388.14444, found 388.14438.

10-(4-(2-chloroquinazolin-4-yl)phenyl)-10*H*-phenoxazine (2Cl-QZ): Prepared according to the same procedure as 2H-QZ but using equimolar 2,4-dichloroquinazoline. The residue was purified by column chromatography on silica gel (eluent: dichloromethane = 1:1) to afford the product as yellow solid (236 mg, yield: 56%). ^{1}H NMR (400 MHz, $CDCl_3$-*d* + TMS, 298 K) δ [ppm]: 8.22 (d, *J* = 9.1 Hz, 1H), 8.10 (d, *J* = 8.5 Hz, 1H), 8.07-7.96 (m, 3H), 7.71 (ddd, *J* = 8.3, 6.9, 1.2 Hz, 1H), 7.65-7.53 (m, 2H), 6.82-6.48 (m, 6H), 6.07 (d, *J* = 1.5 Hz, 2H). ^{13}C NMR (100 MHz, $CDCl_3$-*d*, 298 K) δ [ppm]: 170.50, 157.02, 153.16, 143.98, 141.59, 135.95, 135.18, 133.89, 132.91, 131.41, 128.36, 127.14, 123.31, 121.80, 121.46, 115.70, 113.38.

10-(4-(2-phenylquinazolin-4-yl)phenyl)-10*H*-phenoxazine (2Ph-QZ): To a mixture of 2Cl-QZ (406 mg, 1.0 mmol), 4,4,5,5-tetramethyl-2-phenyl-1,3,2-dioxaborolane (244 mg, 1.2 mmol), potassium carbonate (276 mg, 2 mmol) and Pd(PPh_3)$_4$ (10 mg, 0.01 mmol) was added 20 mL of degassed toluene, 10 mL of degassed ethanol and 10 mL of degassed water. After stirring at 110 °C under an argon atmosphere for 24 h, the mixture was cooled down to room temperature and extracted with 3 × 40 mL of chloroform. The collected organic phase was washed with brine and dried with anhydrous Na_2SO_4. After removal of the solvent, the residue was purified by column chromatography on silica gel (eluent: petroleum/dichloromethane = 1:1, v/v) to afford the product as a greenish-yellow powder (306 mg, yield: 66%). ^{1}H NMR (400 MHz, $CDCl_3$-*d*, 298 K) δ [ppm]: 8.73 (dd, *J* = 8.0, 1.6 Hz, 2H), 8.22 (d, *J* = 7.8 Hz, 1H), 8.20 (d, *J* = 7.8 Hz, 1H), 8.15 (d, *J* = 8.3 Hz, 2H), 7.95 (ddd, *J* = 8.3, 6.9, 1.2 Hz, 1H), 7.71-7.50 (m, 6H), 6.80-6.59 (m, 6H), 6.12 (dd, *J* = 7.4, 1.9 Hz, 2H). ^{13}C NMR (100 MHz, $CDCl_3$-*d*, 298 K) δ [ppm]: 167.53, 160.36, 152.29, 143.98, 140.71, 138.05, 137.76, 134.10, 133.85, 133.04, 131.09, 130.70, 129.42, 128.67, 127.35, 126.71, 123.34, 121.66, 121.52, 115.63, 113.44. HRMS (m/z): calcd for $C_{32}H_{22}N_3O^+$ $[M + H]^+$ 464.1757, found 464.1760.

XYP-2. HRMS (ESI) m/z calcd for $C_{32}H_{22}N_3O^+$ $(M+H)^+$ 464.17574, found 464.17599.

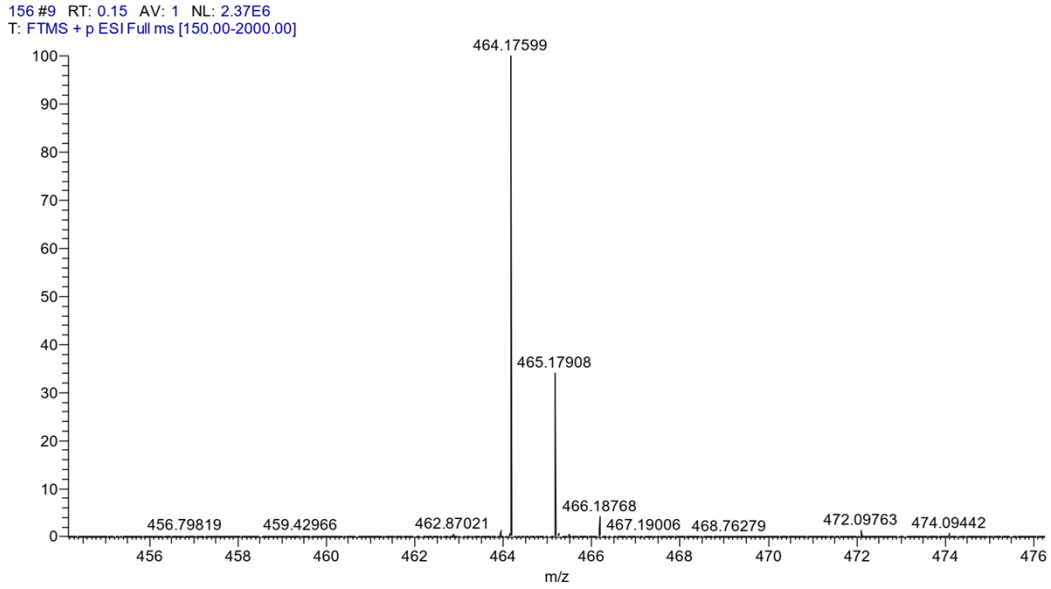

Fig. S2 HRMS (ESI) m/z calcd for $C_{32}H_{22}N_3O^+$ $(M+H)^+$ 464.17574, found 464.17599.

10-(4-(2-(3,5-di(pyridin-2-yl)phenyl)quinazolin-4-yl)phenyl)-10*H*-phenoxazine (2DPyPh-Qz): Prepared according to the same procedure as 2Ph-QZ but using equimolar 2,2'-(5-(4,4,5,5-tetramethyl-1,3,2-dioxaborolan-2-yl)-1,3-phenylene)dipyridine. The residue was purified by column chromatography on silica gel (eluent: dichloromethane) to afford the product as yellow solid (370 mg, yield: 60%). H NMR (400 MHz, $CDCl_3$-*d*, 298 K) δ [ppm]: 9.40 (d, *J* = 1.7 Hz, 2H), 8.86 (t, *J* = 1.7 Hz, 1H), 8.79 (ddd, *J* = 4.8, 1.7, 0.8 Hz, 2H), 8.28 (d, *J* = 8.2 Hz, 1H), 8.23 (d, *J* = 8.4 Hz, 1H), 8.20-8.16 (m, 2H), 8.04 (d, *J* = 8.0 Hz, 2H), 7.96 (ddd, *J* = 8.4, 6.9, 1.3 Hz, 1H), 7.84 (td, *J* = 7.7, 1.8 Hz, 2H), 7.71-7.59 (m, 3H), 7.38-7.26 (m, 2H), 6.83-6.60 (m, 6H), 6.31-6.06 (m, 2H). ^{3}C NMR (100 MHz, $CDCl_3$-*d*, 298 K) δ [ppm]: 167.32, 159.93, 157.25, 152.12, 149.76, 143.98, 140.69, 140.56, 139.26, 137.73, 136.83, 134.13, 133.87, 133.14, 131.14, 129.52, 128.01, 127.70, 127.46, 126.77,

123.36, 122.42, 121.64, 121.11, 115.61, 113.49. HRMS (m/z): calcd for $C_{42}H_{28}N_5O^+$ $[M + H]^+$ 618.2288, found: 618.2289.

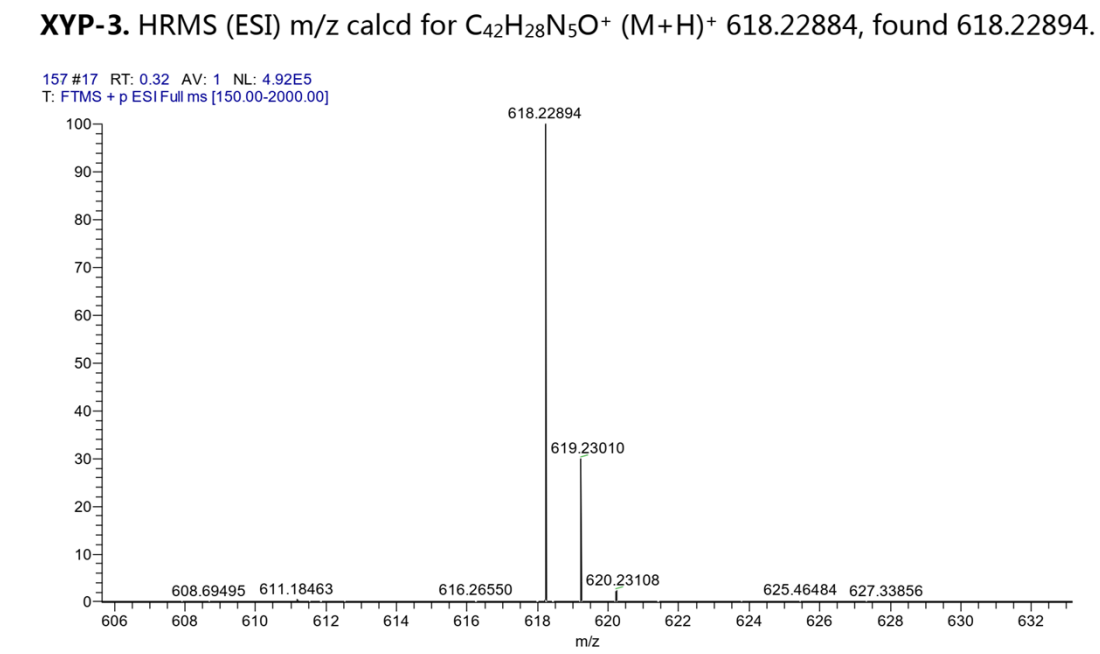

Fig. S3 HRMS (ESI) m/z calcd for $C_{42}H_{28}N_5O^+$ $(M+H)^+$ 618.22884, found 618.22894.

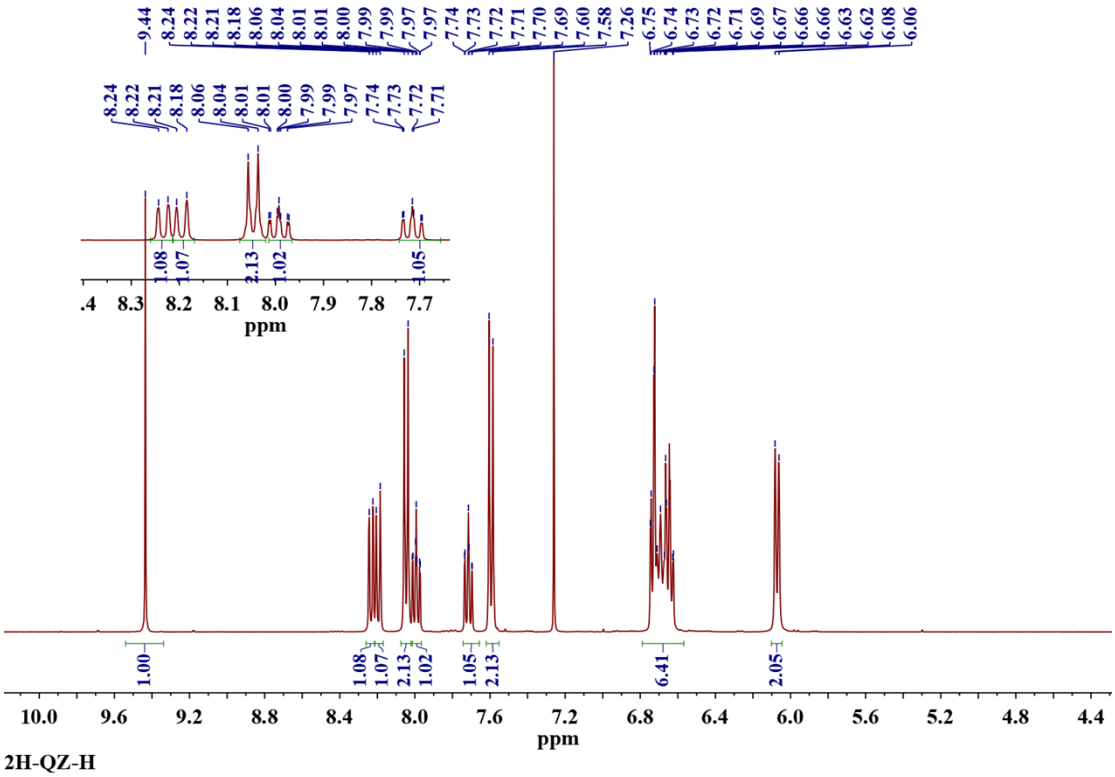

Fig. S4 ^{1}H NMR spectra of 2H-Qz (400 MHz, CD_2Cl_2-d_2 + TMS, 298 K).

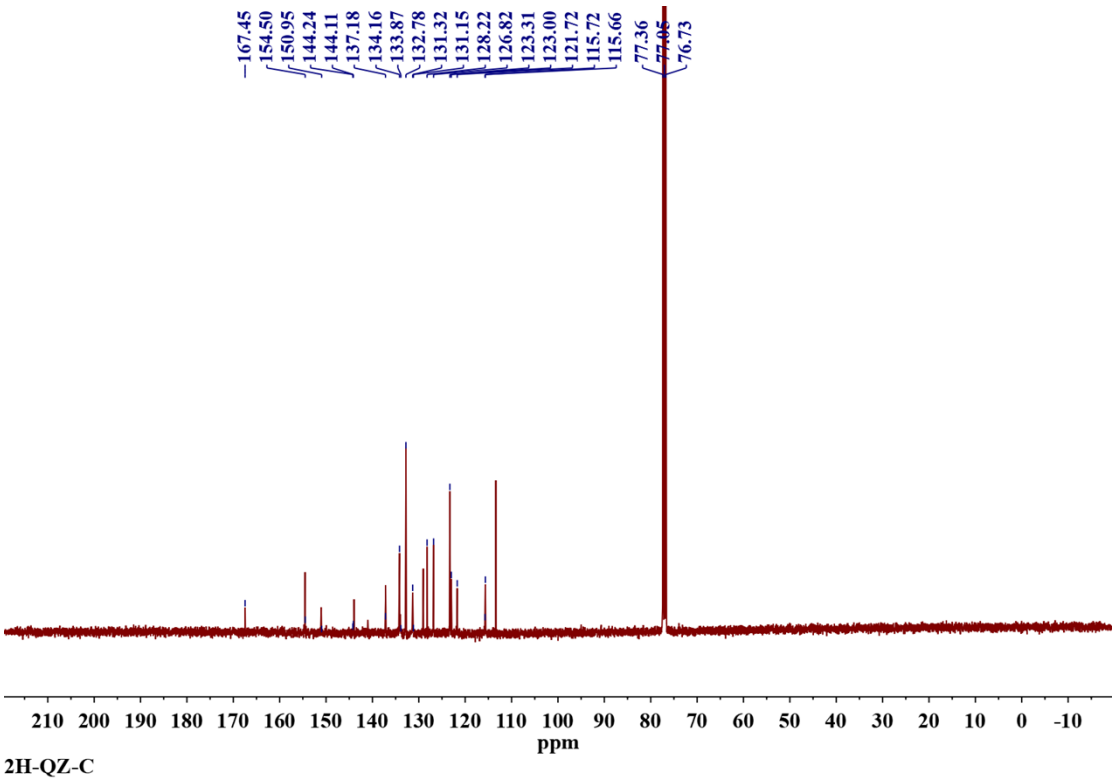

Fig. S5 ^{13}C NMR spectra of 2H-Qz (100 MHz, $CDCl_3$-*d*, 298 K).

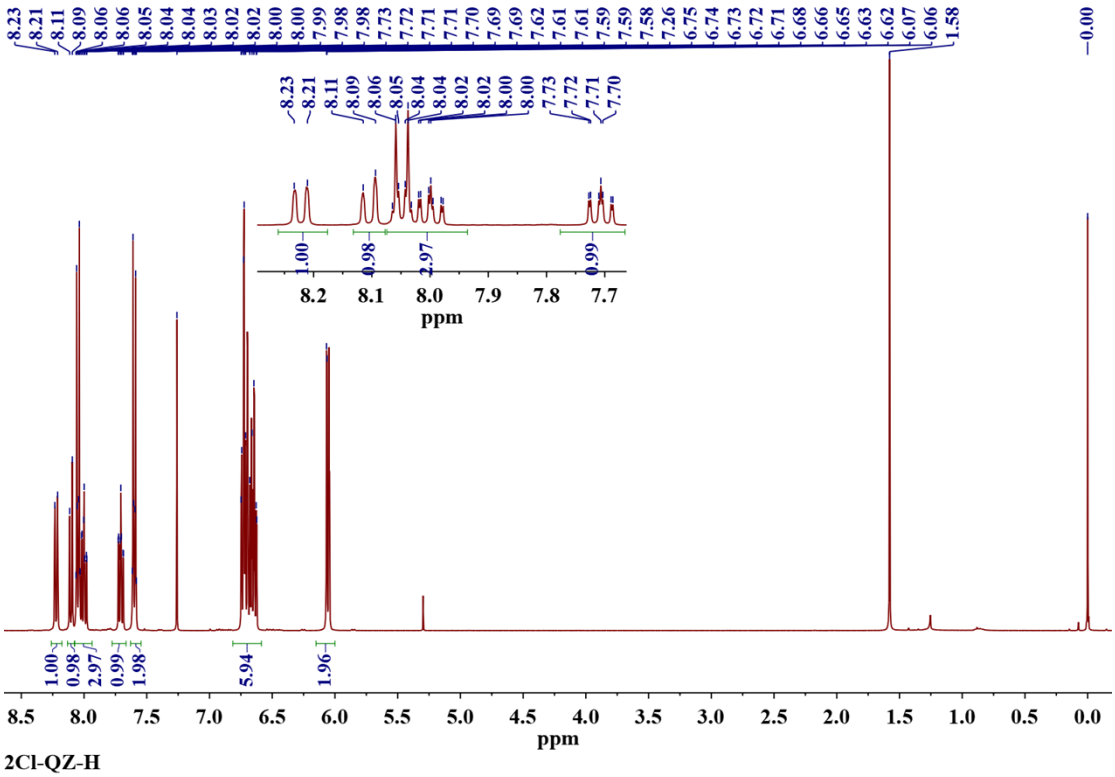

Fig. S6 ^{1}H NMR spectra of 2Cl-Qz (400 MHz, CD_2Cl_2-d_2 + TMS, 298 K)

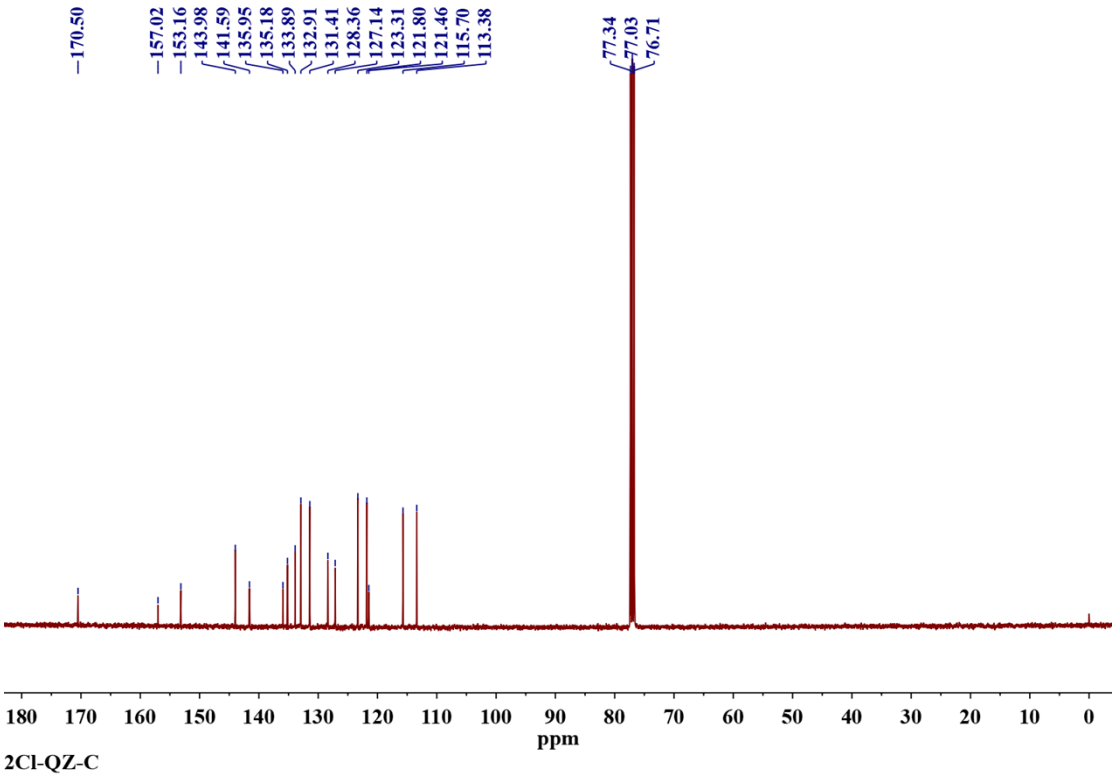

Fig. S7 ^{13}C NMR spectra of 2Cl-Qz (100 MHz, $CDCl_3$-*d*, 298 K).

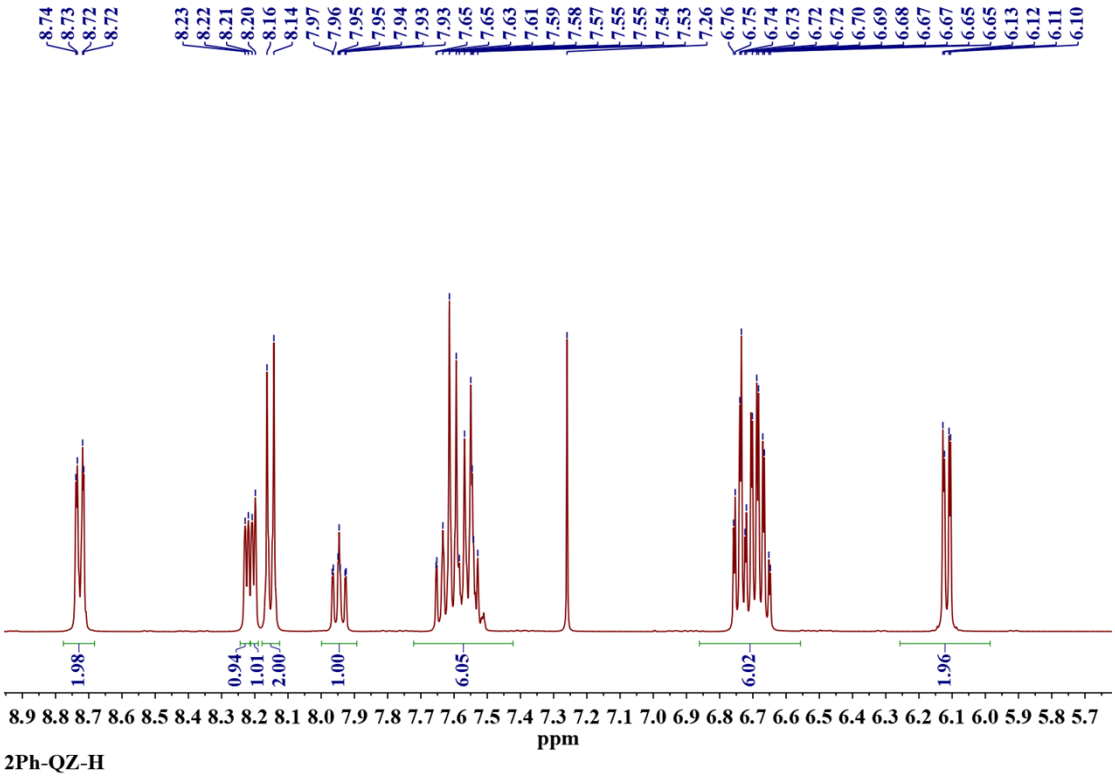

Fig. S8 ^{1}H NMR spectra of 2Ph-Qz (400 MHz, CD_2Cl_2-d_2 + TMS, 298 K).

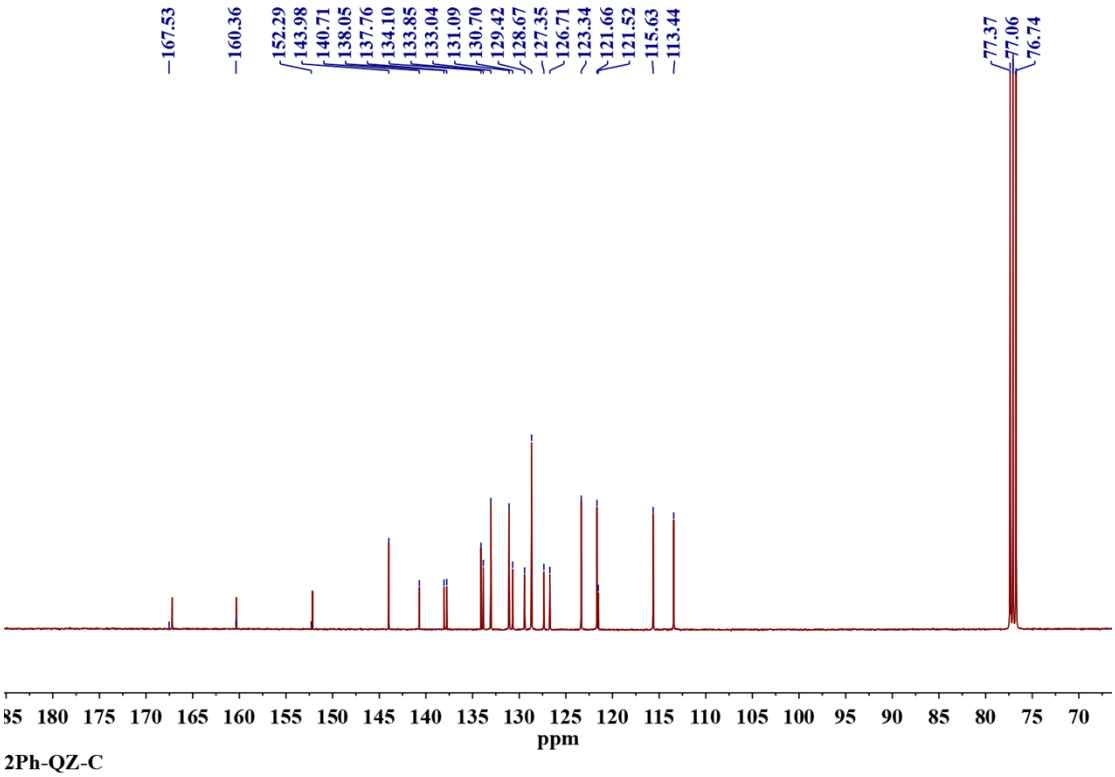

Fig. S9 ^{13}C NMR spectra of 2Ph-Qz (100 MHz, $CDCl_3$-*d*, 298 K).

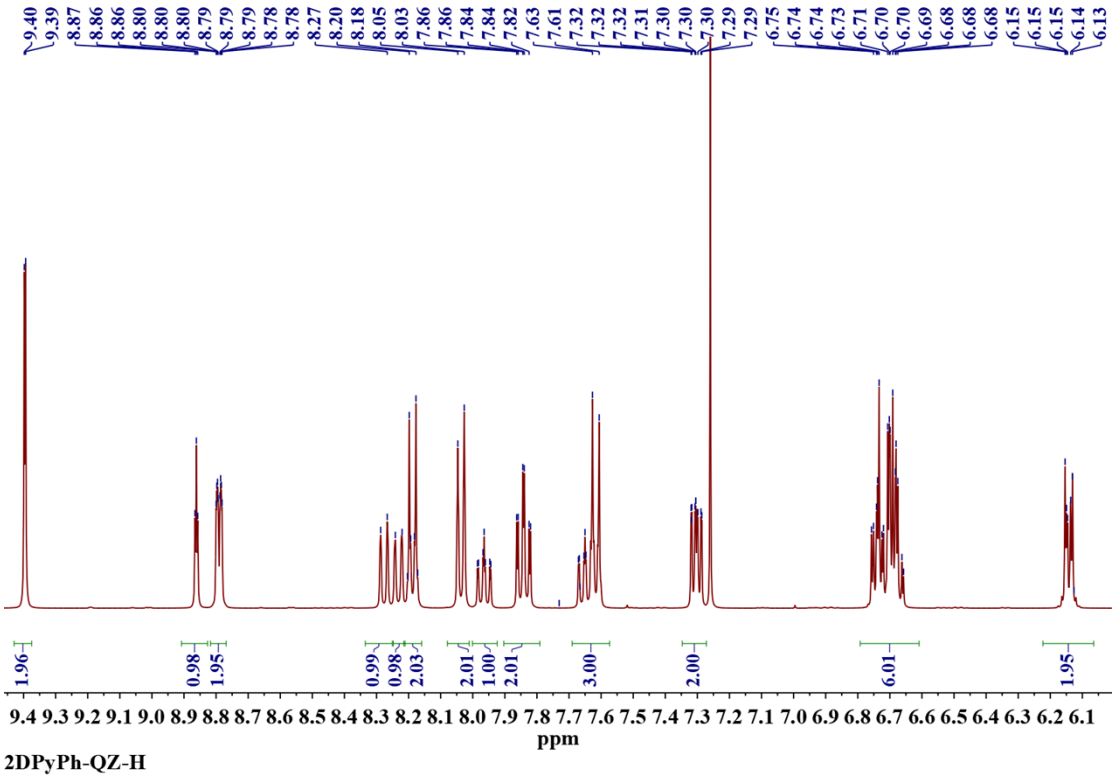

Fig. S10 ^{1}H NMR spectra of 2DPyPh-Qz (400 MHz, CD_2Cl_2-d_2 + TMS, 298 K).

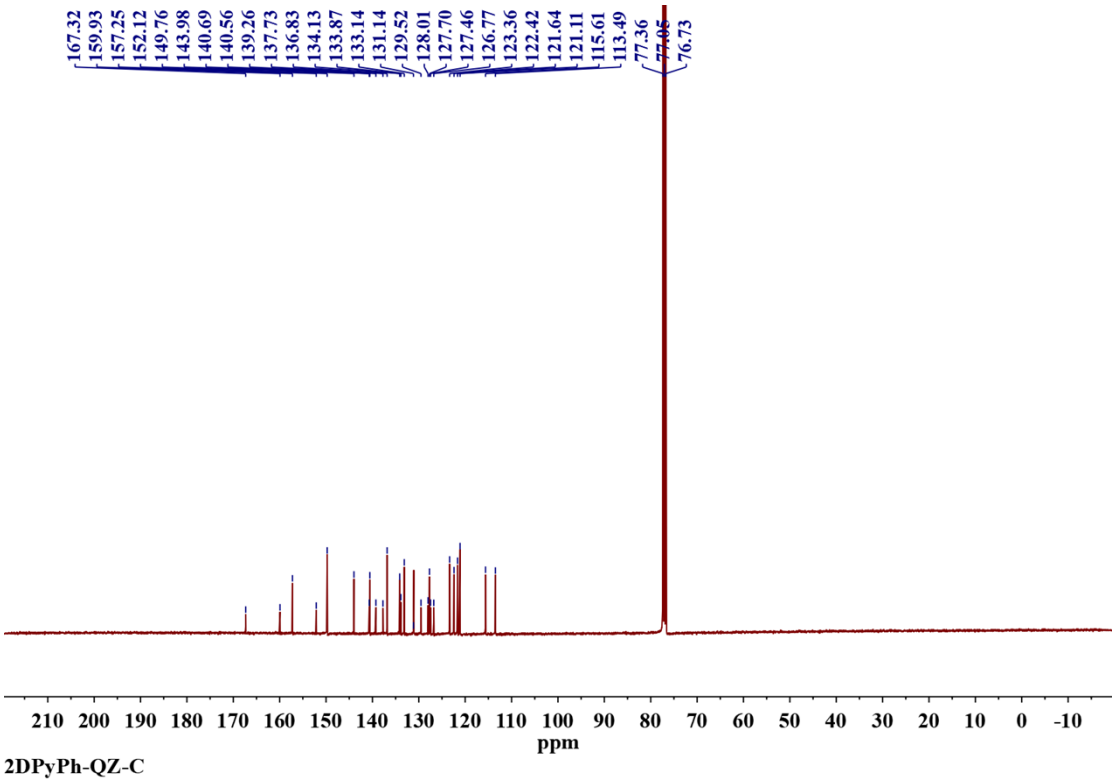

Fig. S11 ^{13}C NMR spectra of 2DPyPh-Qz (100 MHz, $CDCl_3$-*d*, 298 K).

Theoretical calculation:

Ground state structures and FMOs were obtained by B3LYP density functional method with basis set def2-SVP. The dispersion correction was conducted by Grimme's D3 version with BJ damping function.[1, 2] Time-dependent DFT with PBE0 functional and basis set def2-SVP were then performed to further analyse the excited states with the optimized ground state structures. Based on the optimized S_1 state geometries and vibrational normal modes, the nuclear ensemble approach was performed with the Newton-X program.[3] A total of 1000 nuclear configurations were sampled according to the finite-temperature uncorrelated Wigner distribution for room temperature (300 K). TDDFT calculations for $S_1 \rightarrow S_0$ transitions were then performed at the same level to collect the TDMs, oscillator strength, and transition energies of all the configurations.

Arithmetic mean of the *f* and x, y and z components of TDM were then calculated to describe the radiative transition in the dynamic disorder system.[4] The direction of the calculated transition dipole moments (TDMs) and oscillator strengths (*f*'s) were extracted from the simulated S_1 structures (**Figure 4**). S_1 state geometries are optimized at PBE0/def-SVP level with Grimme's D3BJ empirical dispersion correction using TDDFT method. The electronic structures are calculated using the GAUSSIAN16 program.

X-Ray Structural Analysis:

The single crystals of 2Cl-Qz and 2Ph-Qz were achieved from solvent evaporation method from chlorobenzene. Single-crystal X-ray-diffraction data were obtained from a Bruker APEX2 Smart CCD diffractometer through using MoKα radiation (λ = 0.71073 Å) with a $\omega/2\theta$ scan mode at 296 K. Structures of the crystals were solved by direct methods using the APEX2 software. None-hydrogen atoms were refined anisotropically by full-matrix least-squares calculations on F^2 using APEX2, while the hydrogen atoms were directly introduced at calculated position and refined in the riding mode. Drawings were produced using Mercury-3.3. CCDC-2015641 (2Cl-Qz) and CCDC-2015649 (2Ph-Qz) contains supplementary crystallographic data. These data can be obtained free of charge from the Cambridge Crystallographic Data Centre via www.ccdc.cam.ac.uk/data_request/cif.

Photophysical Characterization

Synthesized compounds were subject to purification by temperature-gradient

sublimation in a high vacuum before use in subsequent studies. Thin films for photophysical characterization were prepared by thermal evaporation on quartz substrates at 1-2 Å/sec in a vacuum chamber with a base pressure of < 10^{-6} torr. Absorption spectra were characterized by a UV-vis-NIR spectrophotometer (UV-1650 PC or UV-2700, Shimadzu). Photoluminescence (PL) spectra, photoluminescence quantum efficiencies (Φ_{PL}s), and phosphorescence spectra were characterized by a spectrofluorimeter (FluoroMax-P, Horiba Jobin Yvon Inc. or F-4600, Hitachi Inc.). Φ_{PL}s of thin films or dilute solutions were determined using these spectrofluorometers equipped with a calibrated integrating sphere. During the Φ_{PL} measurements, the integrating sphere was purged with pure and dry nitrogen to keep the environment inert. The selected monochromatic excitation light was used to excite samples placed in the calibrated integrating sphere. By comparing the spectral intensities of the monochromatic excitation light and the PL emission, the PL quantum yields were determined. Phosphorescence spectra of thin films or dilute solutions were conducted at 77 K (the liquid nitrogen temperature) by these spectrofluorometers equipped with a microsecond flash lamp as the pulsed excitation source. A 10-ms delay time was inserted between the pulsed excitation and the collection of the emission spectrum. Time-resolved PL (PL decay curves) was measured by monitoring the decay of the intensity at the PL peak wavelength using the time-correlated single-photon counting fluorescence lifetime system, either FluoroCube of Horiba Jobin Yvon Inc. having nanosecond pulsed light excitation from a 300-nm UV light-emitting diode as the excitation source. The samples were placed in a vacuum cryostat chamber with the

temperature control.

Determination of the emitting dipole orientation of an emitting layer:

To determine emitting dipole orientation of an emitting film, angle-resolved and polarization-resolved PL measurements were performed. The sample consisted of a fused silica substrate with the 30-nm-thick film doped with emitters. The sample was attached to a fused silica half-cylinder prism by index matching liquid. The excitation of the samples was performed with the 325-nm line of the continuous-wave He:Cd laser with a fixed excitation angle of 45o. The emission angle was changed by use of an automatic rotation stage. The spectra were resolved by utilization of a p-polarizing filter and measured by a fiber optical spectrometer.

Analysis of rate constants

The rate constants were analyzed according to the literature method with the assumption that $k_{RISC} >> k_{r,T}+k_{nr,T}$,[5] i.e. almost complete harvesting of triplet excitons to singlets (thus Φ_{RISC}~100%) as suggested by EQE analysis. Where k_{RISC}, $k_{r,T}$ and $k_{nr,T}$ represent the rate constants of the RISC process, the radiative decay and non-radiative decay from T_1 to S_0 states, respectively. The rate constant of radiative decay from S_1 to S_0 states ($k_{r,S}$), the rate constant of non-radiative decay ($k_{nr,S}$) and k_{RISC} can be obtained:

$$k_{r,S} = \Phi_p k_p + \Phi_d k_d \approx \Phi_p k_p \quad \text{(S1)}$$

$$k_{nr,S} = \frac{1 - \Phi_{PL}}{\Phi_{PL}} k_{r,S} \quad \text{(S2)}$$

$$k_{RISC} \approx \frac{k_p k_d \Phi_{PL}}{k_{r,S}} \quad \text{(S3)}$$

$$k_{ISC} \approx \frac{k_p k_d \Phi_d}{k_{RISC} \Phi_p} \quad \text{(S4)}$$

$$\Phi_{ISC} = \frac{k_{ISC}}{k_{r,S} + k_{ISC} + k_{nr,S}} \quad \text{(S5)}$$

Where k_p and k_d represent the decay rate constants for prompt and delayed fluorescence, respectively. They can be experimentally determined from prompt and delayed fluorescence decay time constants (τ_p and τ_d) with a reciprocal relationship. Φ_p and Φ_d represent quantum yields for the prompt and delayed fluorescence components. With Φ_p, Φ_d, τ_p and τ_d experimentally determined from typical Φ_{PL} and transient PL characteristics, $k_{r,S}$, $k_{nr,S}$, k_{RISC} and Φ_{ISC} can be calculated by equations S1-S5.

Device fabrication and measurement

Except for the TADF emitters, the other organic materials used in experiments were purchased from Lumtec, Inc. All compounds were subjected to temperature-gradient sublimation under high vacuum before use. OLEDs were fabricated on the ITO-coated glass substrates with multiple organic layers sandwiched between the transparent bottom indium-tin-oxide (ITO) anode and the top metal cathode. All material layers were deposited by vacuum evaporation in a vacuum chamber with a base pressure of $\leq 10^{-6}$ torr. The deposition system permits the fabrication of the complete device structure in a single vacuum pump-down without breaking vacuum. The deposition rate of organic layers was kept at 0.1-0.2 nm/s. The doping was conducted by co-evaporation from separate evaporation sources with different evaporation rates. The active area of the device is 1 x 1 mm^2, as defined by the shadow mask for cathode deposition. The current-voltage-brightness (I-V-L) characterization of the light-

emitting devices was performed with a source-measurement unit (SMU) and a spectroradiometer (DMS 201, AUTRONIC-MELCHERS GmbH). EL spectra of devices were collected by a calibrated CCD spectrograph. The external quantum efficiencies of devices were determined by collecting the total emission fluxes with a calibrated integrating-sphere measurement system and by measuring the angular distribution of the emission spectra and intensities.

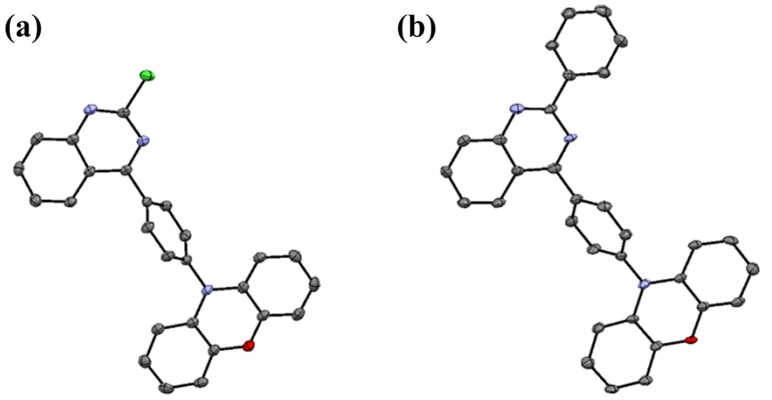

Fig. S12 Single crystal structures of (a) 2Cl-Qz and (b) 2Ph-Qz

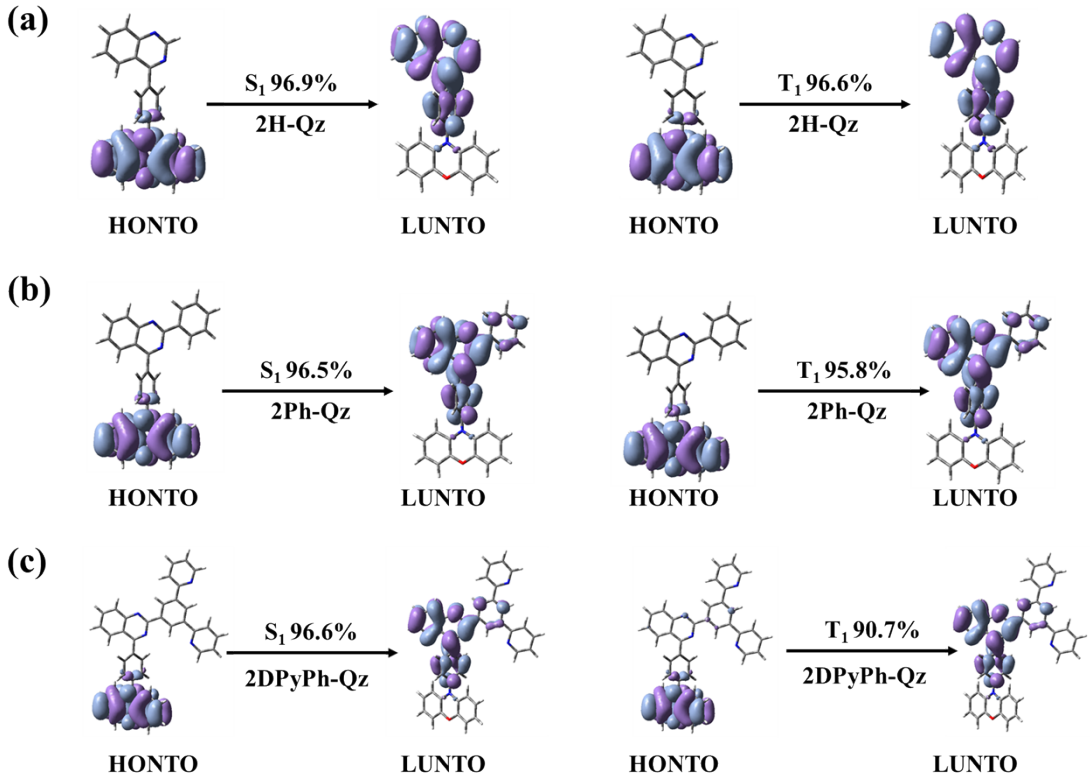

Fig. S13 The HONTO and LUNTO of the S_1 and T_1 state for (a) 2H-Qz, (b) 2Ph-Qz, and (c) 2DPyPh-Qz

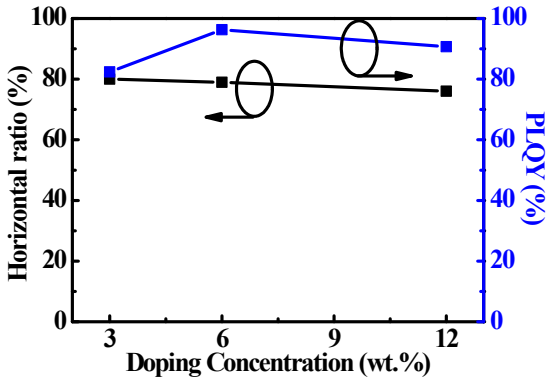

Fig. S14 The Horizontal ratio and PLQYs of 2DPyPh-Qz doped in mCPCN with different doping concentrations.

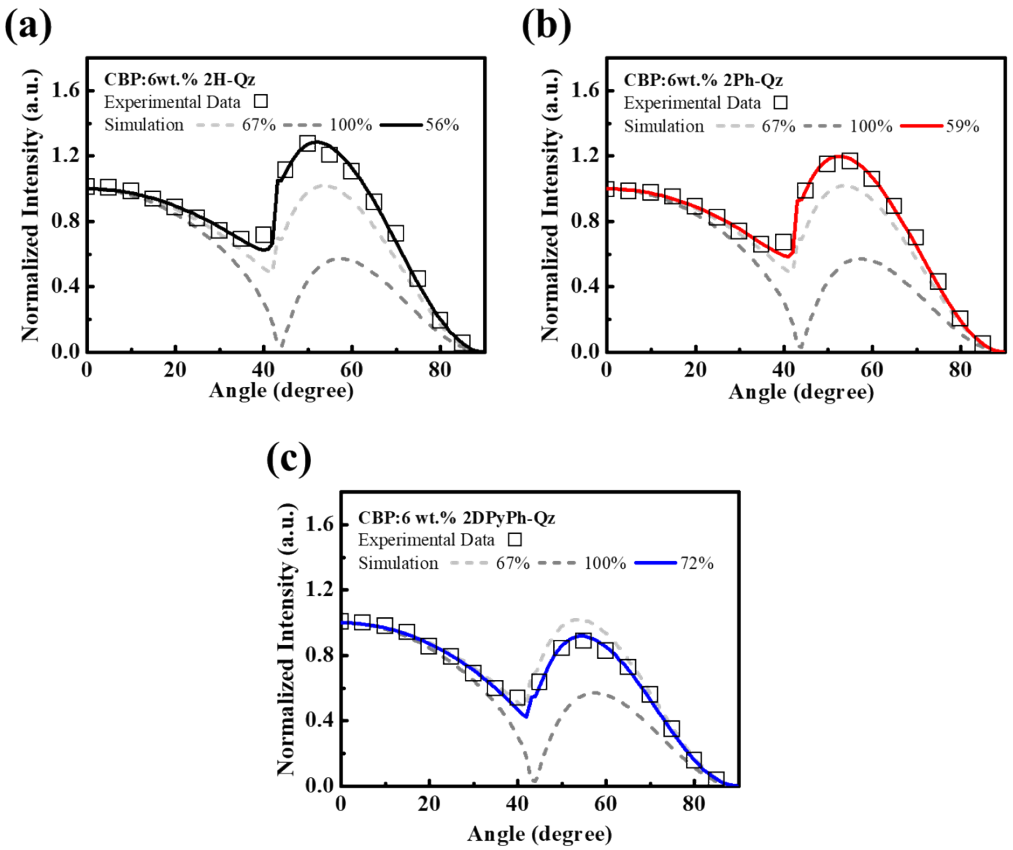

Fig. S15 Measured (symbols) *p*-polarized PL intensity (at PL peak wavelength) of different emitting layers as a function of the emission angle for (a) CBP: 6 wt% 2H-Qz, (b) CBP: 6 wt.% 2Ph-Qz and (c) CBP: 6 wt.% 2DPyPh-Qz, and simulated curves for the fully horizontal dipole orientation ($\Theta_{//}$ = 100%) and the isotropic dipole orientation ($\Theta_{//}$ = 67%).

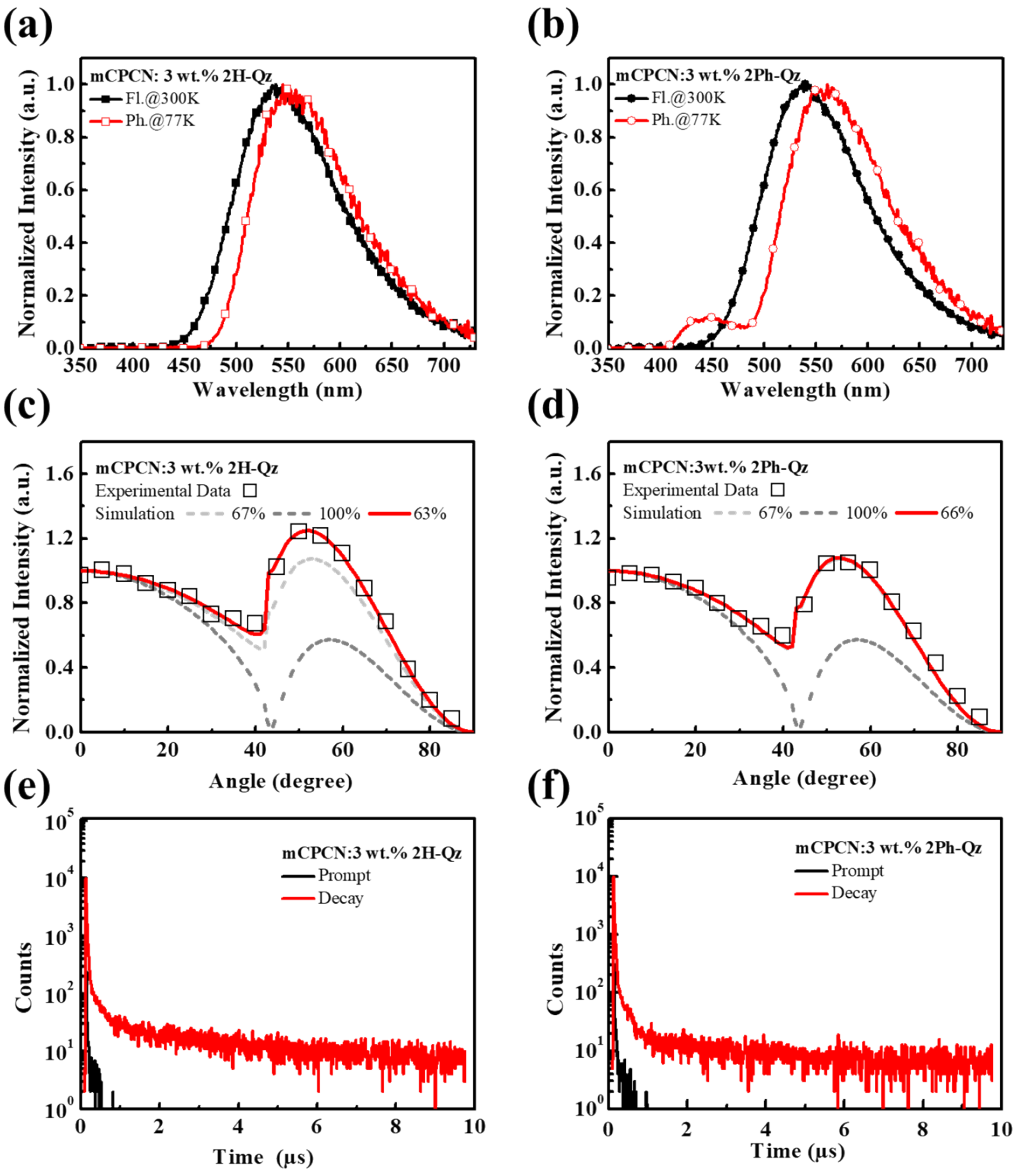

Fig. S16 (a), (b) Normalized fluorescence (300 K) and phosphorescence (77 K) spectra (c), (d) Measured (symbols) *p*-polarized PL intensity (at PL peak wavelength) of different emitting layers as a function of the emission angle (e), (f) Transient PL curves of 2H-Qz and 2Ph-Qz doped into mCPCN films with 3 wt.%.

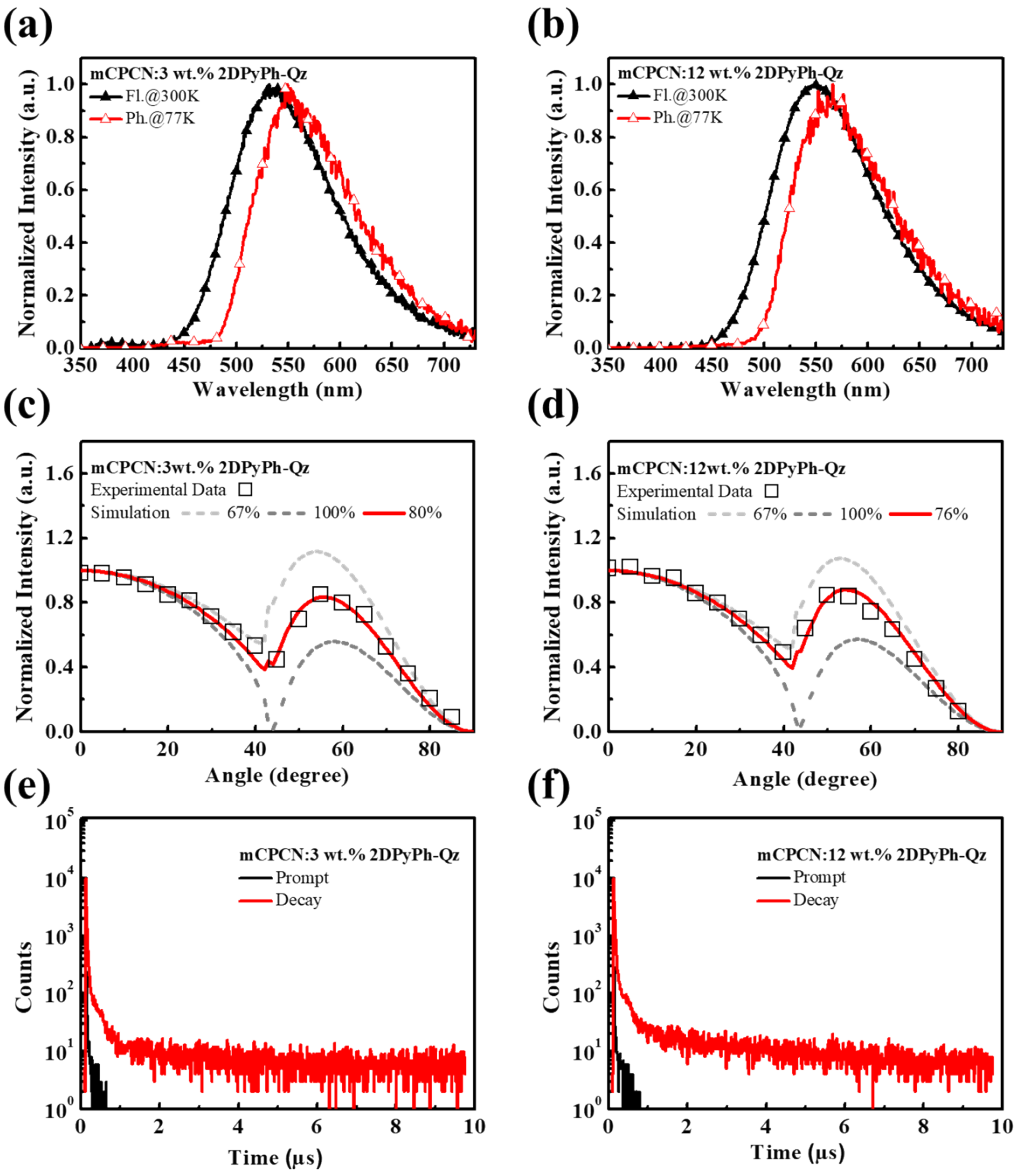

Fig. S17 (a),(b) Normalized fluorescence (300 K) and phosphorescence (77 K) spectra (c),(d) Measured (symbols) *p*-polarized PL intensity (at PL peak wavelength) of different emitting layers as a function of the emission angle (e),(f) Transient PL curves of 2DPyPh-Qz doped into mCPCN films with 3 wt.% and 12 wt.%.

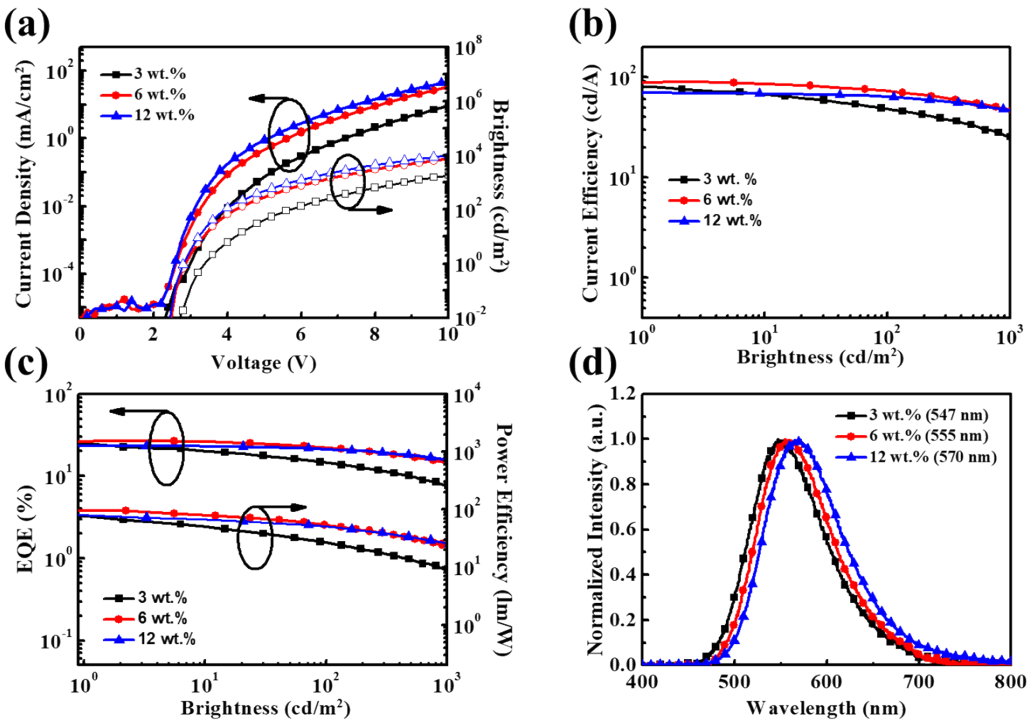

Fig. S18 (a) Current density–voltage–luminance (*I–V–L*) characteristics, (b) current efficiency, (c) external quantum efficiency and power efficiency, (d) electroluminescence spectra for devices based on 2DPyPh-Qz with different doping concentration.

Table S1. Summary of photophysical properties of different concentrations of 2H-Qz, 2Ph-Qz and 2DPyPh-Qz doped into the mCPCN host.

Compounds	Concentration	$\lambda_{PL}{}^{a}$ /$\lambda_{PHOS}{}^{b}$ [nm]	$S_1/T_1/\Delta E_{ST}{}^{c}$ [eV]	$\tau_p/\tau_d{}^{d}$ [ns/μs]	$\Phi_{PL}{}^{e}$ [%]	$\Theta_{//}$[%]
2H-Qz	3 wt.%	538/545	2.70/2.57/0.13	21.4/1.66	92	60
	6 wt.%	551.5/563	2.67/2.56/0.11	23.0/1.07	93	63
2Ph-Qz	3 wt.%	540.5/561	2.66/2.51/0.15	18.6/0.40	91	66
	6 wt.%	541.5/558	2.72/2.50/0.22	20.5/0.41	91	66
2DPyPh-Qz	3 wt.%	531.5/549	2.70/2.55/0.15	17.4/0.46	82	80
	6 wt.%	539.5/557	2.67/2.48/0.19	21.4/0.68	96	79
	12 wt.%	550.5/566	2.65/2.50/0.15	21.7/0.60	91	76

[a] Fluorescence maximum wavelength at 300 K; [b] Phosphorescence maximum wavelength at 77 K; [c] Calculated from the onset wavelengths of fluorescence (77 K) and phosphorescence (77 K) spectra of three emitters in the mCPCN and energy gap between lowest singlet and triplet states; [d] Lifetime of the prompt component and delayed component in transient PL; [e] Photoluminescence quantum yield measured in the mCPCN host under degassed condition at 300 K; [f] Horizontal dipole ratio measured in doped films.

Table S2. The summary of EL characteristics of different concentrations of 2DPyPh-Qz doped into the mCPCN host.

Concentration	V_{on}[a][V]	EL_{peak}[nm]	CIE (x, y)	CE[b][cd A^{-1}]	PE[c][lm W^{-1}]	EQE[d][%]
3 wt.%	3.4	547	(0.40,0.56)	81.2,48.4,25.6	76.6,26.7,9.2	24.5,14.6,7.7
6 wt.%	2.8	555	(0.43,0.55)	89.9,72.7,47.4	96.5,54.2,23.6	27.5,22.3,14.5
12 wt.%	2.8	570	(0.46,0.52)	70.8,63.5,46.8	79.5,50.7,25.6	23.9,21.4,15.8

[a] The turn-on voltage recorded at a brightness of 1 cd m^{-2}. Maximum value, values at 100 and 1000 cd m^{-2} of [b] current efficiency; [c] power efficiency; and [d] external quantum efficiency.

References

1 S. Grimme, J. Antony, S. Ehrlich and H. Krieg, *J. Chem. Phys.*, 2010, **132**, 154104.
2 S. Grimme, S. Ehrlich and L. Goerigk, *J. Comput. Chem.*, 2011, **32**, 1456.
3 M. Barbatti, M. Ruckenbauer, F. Plasser, J. Pittner, G. Granucci, M. Persico and H. Lischka, *WIREs Comput. Mol. Sci.*, 2014, **4**, 26.
4 W. Zeng, S. Gong, C. Zhong and C. Yang, *J. Phys. Chem. C*, 2019, **123**, 10081.
5 K. C. Pan, S. W. Li, Y. Y. Ho, Y. J. Shiu, W. L. Tsai, M. Jiao, W. K. Lee, C. C. Wu, C. L. Chung and T. Chatterjee, *Adv. Funct. Mater.*, 2016, **26**, 7560.